Chalcogenide Letters Vol. 18, No. 1, January 2021, p. 1 - 10

# THE EFFECT OF SOLUTION TEMPERATURE ON CHEMICALLY MANUFACTURED CdS SAMPLES

I. BAL[a], M. C. BAYKUL[b], U. SARAÇ[c,*]
[a]*Vocational School of Health Services, İstanbul Okan University, Opticianry Program, 34959, İstanbul,Turkey*
[b]*Department of Metallurgical and Materials Engineering, Eskisehir Osmangazi University, 26480, Eskişehir, Turkey*
[c]*Department of Science Education, Bartın University, 74100, Bartın, Turkey*

In this paper, CdS samples were chemically coated onto glasses from an aqueous cadmium acetate solution. The resultant samples were analyzed depending on the solution temperature (ST) varied between 65 and 85 °C. Structural analysis confirmed that the ST plays a significant role on the crystallinity. A better crystallization was achieved at the ST of 80 °C. The direct optical band gaps were found to be in the range of 2.18 to 2.42 eV. The ST exhibited a remarkable influence on the surface morphology. Increasing ST from 65 to 80 °C significantly reduced the surface roughness and particle size. The sample chemically produced at the ST of 85 °C exhibited the highest surface roughness and the largest particle size. There was a good relationship between the energy band gap and the surface morphology. Further morphological analysis showed that the ST does not play a role on the surface texture. The highest crystallinity, the lowest surface roughness, the smallest particle size, the lowest band tail energy and the highest optical band gap (2.42 eV) were obtained for the sample manufactured at the ST of 80 °C, indicating that the optimum ST was 80 °C under the applied experimental conditions.

(Received August 2, 2020; Accepted January 11, 2021)

*Keywords:* CdS thin films, Chemical bath deposition, Optical properties, Crystallinity, Roughness, Particle size, Surface texture, Solution temperature

## 1. Introduction

CdS exhibits high refractive index, n–type conductivity, high absorption coefficient, and wide and direct band gap, making it one of the most demanded semiconductor materials [1–4]. Thanks to these features, they are used in a wide variety of industrial and technological applications (window materials in solar cells, optical filters, semiconductor lasers, photo detectors, thin film field effect transistors and gas sensors, etc) [1–6]. In the literature, various manufacturing methods are available to produce CdS films. The chemical bath deposition (CBD) is one of the most attractive and effective methods due to its cost effectiveness, minimum material wastage, reproducibility and simple experimental setup [2, 5, 7]. In the manufacturing process of CdS thin film materials, cadmium sulfate, cadmium acetate, cadmium nitrate, cadmium iodide and cadmium chloride are served as a cadmium source, while the thiourea, sodium thiosulfate and sodium sulfate are employed as a sulfur source [5, 8–13]. In addition, various complexing agents are also introduced to the reaction solution [8, 14–16]. Among the complexing agents, ammonia is commonly used in fabrication process of materials carried out by CBD [2, 3, 8, 12]. It was shown that the concentration of ammonia in the reaction solution plays a significant role on the Cd/S ratio, morphology, microstructure and optical features of the chemically fabricated CdS films [8]. Also, it is well known that the type and concentration of the reactants strongly affected the characteristic properties of the chemically deposited films. A comprehensive study carried out by Khallaf et al. revealed the effects of four different types of cadmium source on CdS films [12]. The influences of thiourea concentration and two types of cadmium source were also studied and it was

* Corresponding author: usarac@bartin.edu.tr

found the crystal structure and optical band gap are significantly affected by these deposition variables [1]. Lee et al. examined the role of the ammonium acetate concentration on CdS samples [17]. When the CBD method is used in manufacturing process of the materials, apart from the type and concentration of the reactants, the parameters (production time, solution pH, stirring speed and ST) should be also controlled to produce high quality semiconductor materials. In particular, the ST has a significant impact on CdS samples grown by CBD technique [7, 9, 18–26]. In these previous studies, cadmium sulfate [9, 18, 19, 21, 22, 25], cadmium chloride [7, 20, 23, 26] and cadmium acetate [24] were used as a cadmium source in the manufacturing process performed at various STs. Based on the literature, it is clear that the effects of ST on CdS materials chemically fabricated from a cadmium acetate solution have not been sufficiently investigated. The crystallinity, optical properties and particle size of the CdS materials chemically produced from a cadmium acetate solution at three different STs of 60, 70 and 90 °C were clearly reported [24]. In this work, therefore, we studied the effect of the ST not only on the crystallinity, optical properties and particle size but also on the S/Cd ratio, roughness and surface texture of the CdS samples chemically fabricated from a cadmium acetate solution.

## 2. Experimental

CdS materials were produced by means of the CBD technique depicted in Fig. 1. To avoid the organic impurities, the cleaning process of the glass substrates was carried out prior to deposition process. The 1 × 1 cm glass substrates purchased from ISOLAB were cleaned in the acetone medium, ethanol medium and distilled water, respectively.

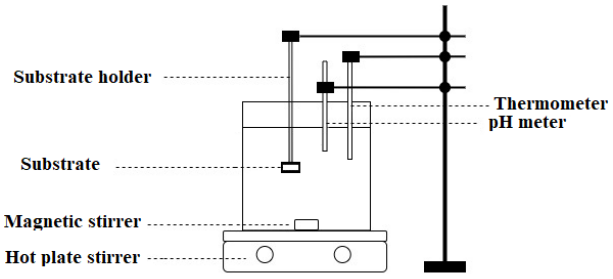


*Fig. 1. CBD system used in the manufacturing process of the CdS samples.*

The solution bath composed of 0.002 M [$Cd(CH_3COO)_2.2H_2O]_2$, 0.03M [$CH_3COONH_4$] and 0.04 M [$CS(NH_2)_2$]. As a first step of manufacturing process, cadmium acetate for providing cadmium ions was dissolved in 100 ml distilled water. Then, thiourea and ammonium acetate were introduced to the bath solution, respectively. The solution was vigorously stirred to achieve homogeneity and the stirring speed was kept constant during deposition process. The solution pH was controlled by adding [$NH_3.H_2O$] and maintained at 10.5. Also, with the addition of [$NH_3.H_2O$] as a complexing agent, the blurry solution became clear. The production time for all samples was 30 minutes and the ST was gradually changed from 65 to 85 °C. After manufacturing process, CdS samples were washed with distilled water and dried in air, and then hold in a closed vessel. Finally, yellowish and good adherent CdS samples were obtained.

The crystallization and crystal structure of the produced samples were examined using a Rigaku SmartLab X–ray diffractometer (XRD). The scan was done in the range of $20^{\circ}$ to $60^{\circ}$ using a Cu–K$\alpha$ radiation. The elemental analysis in atomic percentages (at. %) was performed using an energy dispersive X–ray spectrometer (EDS). The morphological studies were performed using an atomic force microscopy (AFM) in tapping mode (MultiMode V SPM of Veeco) and a scanning electron microscopy (SEM) at ambient temperature and pressure (Tescan MAIA3). An ultraviolet–visible light spectrometer (UV–VIS, Shimadzu UV–1800) was used to examine the optical features.

## 3. Results and discussion

The influence of the ST on the crystal structure and crystallinity was studied using the XRD characterization technique and the recorded XRD patterns are indicated in Fig. 2. It is clearly noticed from the XRD patterns that the films exhibit a large bump located in the low diffraction angles irrespective of the ST, reflecting the formation small crystallites embedded in an amorphous structure [5, 18]. Chemically deposited CdS thin films can be cubic or hexagonal with respect to the deposition parameters applied in the fabrication process of the films [27]. As also reported in former studies [5, 17, 18, 27, 28], the reflections of cubic CdS structure coincide with those of hexagonal CdS structure. Therefore, it is difficult to distinguish whether the resultant CdS samples are cubic or hexagonal. The XRD patterns reveal the presence of the (111) reflection of the cubic CdS structure or (200) reflection of the hexagonal CdS structure located at the angular position of about 2θ=26.7°. In addition, weak C(220) and C(311) or H(110) and H(112) reflections are observed at the angular positions of about 2θ=44° and 2θ=52°, respectively. However, regardless of the ST, the intensity of the C(111) or H(200) diffraction peak is stronger compared to that of other peaks, indicating that the [111] direction or [200] direction is the preferred orientation, respectively. In addition, a change in the ST strongly affects the diffraction peak intensities. As the ST is increased from 65 to 80 °C, the C(111) or H(200) diffraction peak intensity increases strongly, and then it reaches to its lowest level at the ST of 85 °C. Consequently, a better crystallization is observed at the STs of 70 and 80 °C. The other films fabricated at the STs of 65 and 85 °C show a poor crystallinity. Higher degree of crystallinity observed at the STs of 70 and 80 °C can be ascribed to a decrease in the amount of structural defects in the samples acting as scattering centers [29].

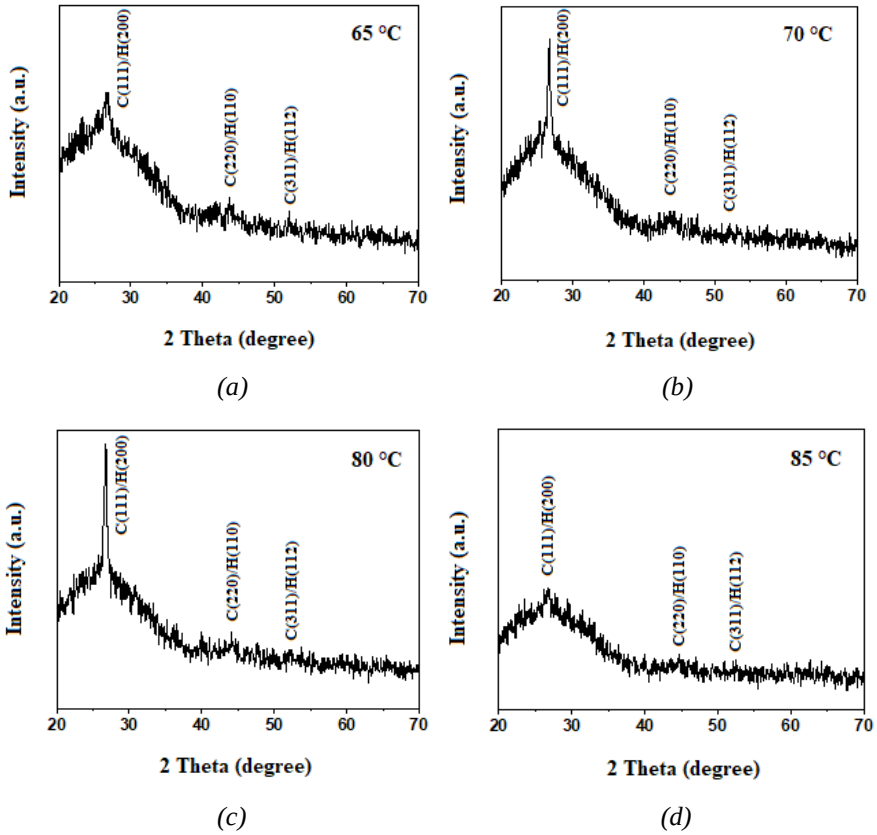


*Fig. 2. XRD patterns of the CdS thin films chemically deposited at a) 65 °C, b) 70 °C, c) 80 °C, d) 85 °C.*

The elemental analysis was done by means of the EDS measurements. As an example, the EDS spectrum for the sample chemically produced at the ST of 80 °C is demonstrated in Fig. 3a. It is observed that all CdS thin films contain the Cd and S elements irrespective of the ST. However, the Ca, Mg, Na, C, O and Si elements are also detected. These elements appeared in the EDS spectra of CdS thin films originate from activated carbon and glass substrate. After eliminating the disturbance of other elements, the atomic percentages of Cd and S are estimated. Fig. 3b reveals that the Cd and S percentages are very close, indicating that the ratio of S/Cd approaches unity. These results indicate a very homogenous film formation, particularly for the films deposited at the STs of 70 and 80 °C. On the other hand, as distinctly noticed from the Fig. 3b, the percentage of S is found to be always slightly higher than that of the Cd irrespective of the ST, which is attributed to the deficiency in cadmium. In an earlier study, the formation of the cadmium deficiency in manufacturing process was explained and related to the ammonia concentration [8].

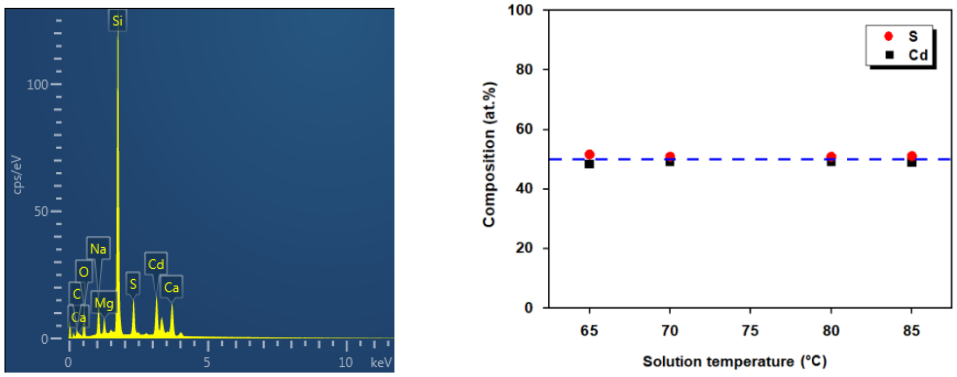


*(a)* *(b)*

*Fig. 3. (a) EDS spectrum of the CdS sample chemically produced at the ST of 80 °C; (b) variation of the Cd and S percentages in the samples with respect to the ST.*

Morphological analysis was performed using both SEM and AFM measurements. The recorded SEM and AFM micrographs are shown in Fig. 4 and 5, respectively. The crack and pinhole–free morphological structure is achieved for all CdS thin films regardless of the ST. However, the properties of the surface morphology were remarkably influenced by the ST. From the SEM micrograph depicted in Fig. 4a, it is clearly seen that the surface morphology exhibits a flake–like structure at the ST of 65 °C. Similar flake–like structure has been also reported in chemically produced CdS thin films [27]. At the ST of 70 °C, although the flake–like structure is still observed at the upper part, the occurrence of the grainy morphology is clearly noticed at the bottom part (Fig. 4b). Furthermore, the size of flake–like structures considerably decreases when the ST is increased from 65 to 70 °C. As distinctly noticed from the Fig. 4c, the flake–like structures almost disappear and the grainy morphology becomes clear at the ST of 80 °C. With a further increase in the ST to 85 °C, the flake–like structures again appear (Fig. 4d). Consequently, the surface morphology consisting of only flake–like structures is obtained at the STs of 65 and 85 °C, while the grainy morphology with and without flake–like structures is obtained at the STs of 70 and 80 °C, respectively.

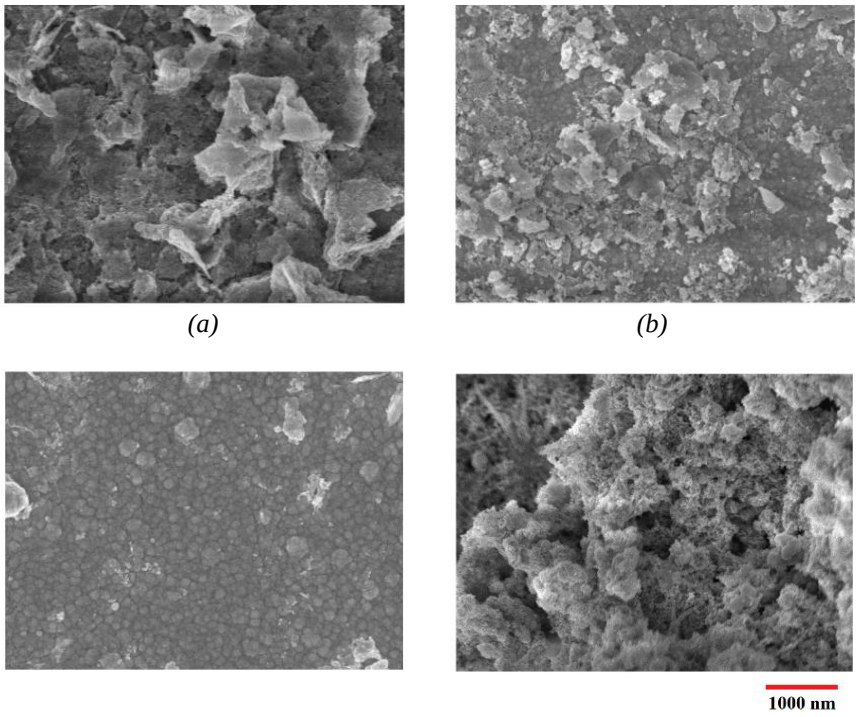


*(a)* *(b)* *(c)* *(d)*

*Fig. 4. SEM micrographs of the chemically fabricated CdS samples a) 65 °C, (b) 70 °C, c) 80 °C and d) 85 °C, respectively.*

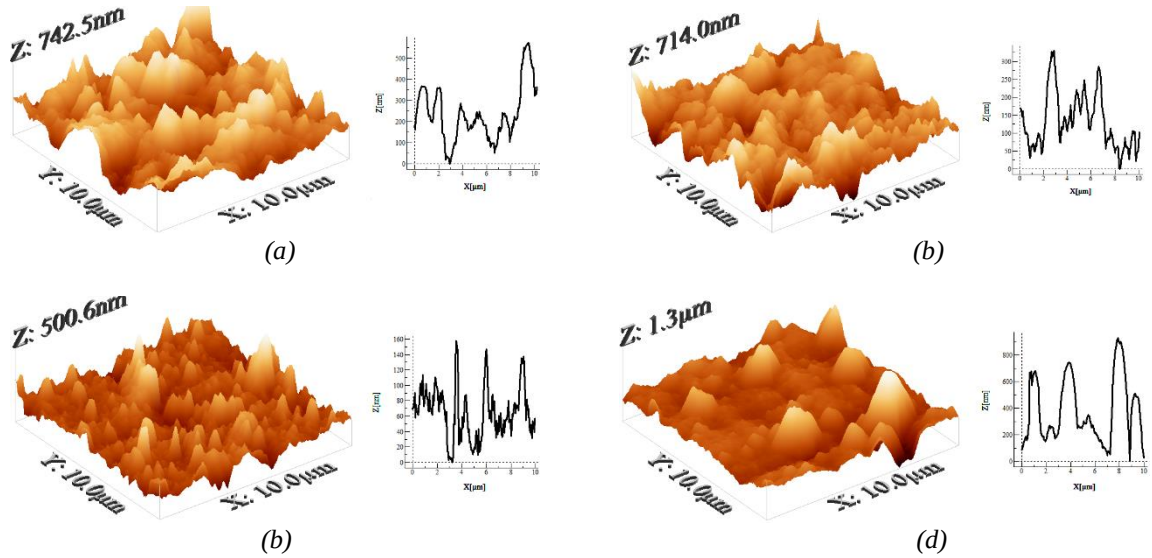


*(a)* *(b)* *(b)* *(d)*

*Fig. 5. AFM micrographs of the chemically grown CdS samples a) 65 °C, b) 70 °C, c) 80 °C and d) 85 °C, respectively.*

The optical performances of materials can be related to the surface roughness [30–32]. AFM is a useful method to provide a knowledge about the morphological features of the materials such roughness, surface texture and particle size. The surface roughness values and line profile scans were obtained by means of the WSxM software package (version 5.0 Develop 8.2) [33]. From the AFM micrographs (Fig. 5), it is observed that the films have agglomerated particles of various sizes and they are randomly distributed over the surface. The line profile scans confirm

that increasing ST from 65 to 80 °C gives rise to a strong decrease in the size of the agglomerated particles in both vertical and horizontal directions. The largest agglomerated particle sizes are detected at the ST of 85 °C. The results obtained from the AFM analysis are consistent with those of the SEM analysis. A decrease or an increase in the agglomerated particle size according to the ST can be ascribed to a decrement or an increment in the nucleation sites. An increase in the nucleation sites on the glass substrate surface increases the number of the particles and therefore gives rise to a decrement in the particle size. Depending on the ST, the changes in the particle size in both vertical and horizontal directions affect the surface roughness values. The surface roughness values are shown in Table 1 against the ST. As clearly noticed from Table 1, there is a considerable reduction in the roughness values as the ST is increased from 65 to 80 °C. The film chemically deposited at the ST of 85 °C exhibits the roughest surface morphology. Consequently, it is clear that the surface morphologies are directly dependent on the ST. A similar relationship between the ST and the surface roughness, which is revealed in this study, was also reported for the CdS nanofilms chemically coated from a chloride bath in a former work [20].

The texture direction index and isotropy index parameters were determined with the help of Mountains®8 software to analyze the changes in the surface texture depending on the ST [34]. The texture direction index parameter is approximate to zero or one for a surface with and without a predominant direction, respectively [35–37]. On the other hand, the strength of the surface texture is evaluated according to the value of the isotropy index parameter [35, 36, 38]. Furthermore, the isotropy index parameter is approximate to zero for a surface displaying an anisotropic property, while it is approximate to one for a surface structure having a spatially isotropic feature [35–38]. The obtained values of the texture direction index and isotropy index parameters are listed in Table 1. Based on the values given in Table 1, it is concluded that the temperature of the solution used in the manufacturing process does not play a role on the nature of the surface texture. All CdS samples have a spatially isotropic surface texture.

*Table 1. Root–mean–square (RMS) roughness, average roughness, isotropy index and texture direction index values of the chemically fabricated CdS samples for various STs.*

| ST (°C) | Roughness (nm) | | Isotropy index | Texture direction index |
|---|---|---|---|---|
| | RMS | Average | | |
| 65 | 110.2 | 89.4 | 0.5690 | 0.5352 |
| 70 | 80.4 | 62.7 | 0.6658 | 0.6290 |
| 80 | 51.5 | 36.9 | 0.7964 | 0.6027 |
| 85 | 139.3 | 94.2 | 0.6346 | 0.5612 |

To investigate the optical features, absorbance measurements were carried in the wavelength range of 400 to 700 nm. The optical band gaps were estimated from the absorbance measurements using Tauc's plot. According to Tauc's relation, the correlation between the absorption coefficient ($\alpha$) and the photon energy ($h\nu$) for near–edge absorption in semiconducting materials is expressed as [39, 40];

$$\alpha h\nu = A(h\nu - E_g)^n$$

where $A$ is a constant and $E_g$ is the optical band gap. In this equation, n is taken as 1/2 for an allowed direct band gap. Thus, the direct optical band gaps were determined by extrapolating the linear portions of the $(\alpha h\nu)^2$ versus $h\nu$ plots. The plots and estimated optical band gap values are illustrated in Fig. 6. The optical band gap varies between 2.18 and 2.42 eV depending on the ST. The optical band gap values of our CdS samples are consistent with the values reported in former studies [3, 4, 9, 10, 12, 13, 19, 21, 41]. As distinctly seen from Fig. 6, the optical band gap increases from 2.30 to 2.42 eV with increasing ST from 65 to 80 °C. However, the optical band gap significantly decreases from 2.42 to 2.18 eV when the ST is increased from 80 to 85 °C. Furthermore, it is observed that the optical band gap is compatible with the surface roughness. Fig. 7 indicates the correlation between the average roughness and the optical band gap. As clearly

seen from Fig. 7 that there is a good relationship between the band gap and the surface roughness. The sample chemically grown at the ST of 80 °C (85 °C) exhibiting the smoothest (roughest) surface morphology possesses the highest (lowest) optical band gap value.

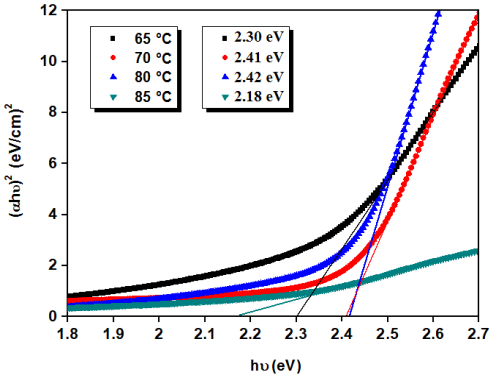


*Fig. 6. Estimation of the optical band gap of chemically produced CdS samples for different STs.*

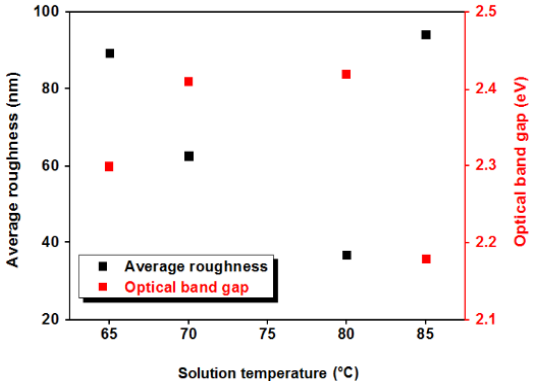


*Fig. 7. Correlation between the average roughness and the optical band gap in chemically fabricated CdS thin films for different STs.*

The band tail energy is an important parameter to evaluate the amount of disordered atoms and defects and a decrease in the band tail energy corresponds to an improvement in the structural disorder [5, 19, 22, 41–45]. The band tail energy can be estimated with the help of absorption coefficient and photon energy near the optical band edge using the exponential equation given below [44, 45],

$$\alpha = \alpha_o \exp(h\nu/E_U)$$

$$\ln\alpha = \ln\alpha_o + (h\nu/E_U)$$

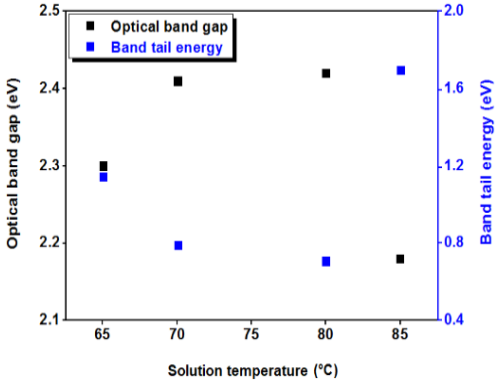


*Fig. 8. Relationship between the optical band gap and the band tail energy in chemically deposited CdS thin films for various ST.*

where $\alpha_o$ is a constant, $E_U$ represents the band tail energy of the localized states in the optical energy gap and $hv$ denotes the incident photon energy. The band tail energy is determined from the slope of the straight line of plotting ln($\alpha$) against ($hv$). The band tail energy values were estimated to be in the range of 0.71 to 1.72 eV. Fig. 8 shows the relationship between the optical band gap and the estimated band tail energy for different STs. The reduction in the band tail energy results in an increment in the optical band gap. This means that the structural disorder and crystallinity are strongly related to the band gap. An improvement in the crystallinity and a decrement in the number of defects and disordered atoms results in the formation of a higher optical band gap at intermediate STs of 70 and 80 °C.

Accordingly, it is concluded that the optical performance of the chemically manufactured CdS samples can be improved by controlling their morphological and structural features. Thus, the CdS sample chemically deposited at intermediate ST of 80 °C having higher crystallinity, lower band tail energy, lower surface roughness and smaller particle size exhibited a higher band gap in comparison to other samples chemically produced under the study. This makes it more suitable for applications.

## 4. Conclusion

To examine the influence of the ST on the crystallinity, S/Cd ratio, optical band gap, surface morphology, particle size, surface roughness and surface texture, the CdS samples were fabricated onto glass substrates from a cadmium acetate solution using CBD method at various STs of 65, 70, 80 and 85 °C. Crack and pinhole–free CdS thin films with good adherence were obtained. Increasing ST from 65 to 80 °C led to a strong improvement in the crystallinity; however, the film deposited at the ST of 85 °C exhibited the worst crystallization. The optical band gap increased from 2.30 to 2.42 eV when the ST was increased from 65 to 80 °C, and then decreased to its minimum value of 2.18 eV as the ST was further increased to 85 °C. The band tail energy values varied between 0.71 and 1.72 eV.

A decrement in the amount of disordered atoms and defects and an improvement in the crystallinity resulted in an increment in the band gap. The samples chemically manufactured at the STs of 65 and 85 °C exhibited a surface morphology consisting of only flake–like structures. However, the films fabricated at the STs of 70 and 80 °C had a grainy morphology with and without flake–like structures, respectively. The particle size and roughness showed a strong dependency on ST. While the agglomerated particle size and roughness decreased as the ST was increased from 65 to 80 °C, the film grown at the ST of 85 °C had the largest agglomerated particle size and the highest surface roughness. However, the ST did not play a role on the surface texture.

All CdS samples showed an isotropic surface texture without a predominant direction. As a result, under the deposition parameters applied in this work, the CdS sample manufactured at 80 °C exhibited higher crystallinity, lower surface roughness, smaller agglomerated particle sizes, lower band tail energy and a higher band gap (2.42 eV) in comparison to other CdS samples, making it more suitable for applications.

**Acknowledgements**

The authors wish to thank Çağdaş Denizli for taking AFM images.

## References

[1] R. Zia, M. Riaz, Q. Ain, S. Anjum, Optik **127**, 5407 (2017).
[2] E. Yücel, S. Kahraman, H.S. Güder, Mater. Res. Bull. **68**, 227 (2015).
[3] E. Yücel, N. Güler, Y. Yücel, J. Alloys Compd. **589**, 207 (2014).
[4] S. Prabahar, M. Dhanam, J. Cryst. Growth **285**, 41 (2005).
[5] S. Hariech, M. S. Aida, J. Bougdira, M. Belmahi, G. Medjahdi, D. Genève, N. Attaf, H. Rinnert, J. Semicond. **39**, 034004 (2018).
[6] A. S. Najm, M. S. Chowdhury, F. T. Munna, P. Chelvanathan, V. Selvanathan, M. Aminuzzaman, K. Techato, N. Amin, MD. Akhtaruzzaman, Chalcogenide Lett. **17**, 537 (2020)
[7] S. Rondiya, A. Rokade, B. Gabhale, S. Pandharkar, M. Chaudhari, A. Date, M. Chaudhary, H. Pathan, S. Jadkar, Energy Procedia **110**, 202 (2017).
[8] Q. Q. Liu, J. H. Shi, Z. Q. Li, D. W. Zhang, X. D. Li, Z. Sun, L. Y. Zhang, S. M. Huang, Physica B **405**, 4360 (2010).
[9] E. Çetinörgü, C. Gümüş, R. Esen, Thin Solid Films **515**, 1688 (2006).
[10] L. Ma, X. Ai, X. Wu, J. Alloys Compd. **691**, 399 (2017).
[11] V. B. Sanap, B. H. Pawar, Chalcogenide Lett. **7**, 227 (2010).
[12] H. Khallaf, I. O. Oladeji, G. Chai, L. Chow, Thin Solid Films **516**, 7306 (2008).
[13] E. Yücel, O. Şahin, Ceram. Int. **42**, 6399 (2016).
[14] M. T. S. Nair, P. K. Nair, J. Campos, Thin Solid Films **161**, 21 (1988).
[15] A. V. Feitosa, M. A. R. Miranda, J. M. Sasaki, M. A. Araújo–Silva, Braz. J. Phys. **34**, 656 (2004).
[16] H. Zhang, X. Ma, D. Yang, Mater. Lett. **58**, 5 (2004).
[17] S. Lee, D. Kim, D. Baek, B. Hong, J. Yi, J. Lee, J. Korean Phys. Soc. **64**, 1566 (2014).
[18] F. Liu, Y. Lai, J. Liu, B. Wang, S. Kuang, Z. Zhang, J. Li, Y. Liu, J. Alloys Compd. **493**, 305 (2010).
[19] H. Moualkia, S. Hariech, M. S. Aida, Thin Solid Films **518**, 1259 (2009).
[20] S. Kumar, P. Sharma, V. Sharma, Phys. Scr. **88**, 045603 (2013).
[21] Y. S. Lo, R. K. Choubey, W. C. Yu, W. T. Hsu, C. W. Lan, Thin Solid Films **520**, 217 (2011).
[22] H. Moualkia, S. Hariech, M. S. Aida, N. Attaf, E. L. Laifa, J. Phys. D: Appl. Phys. **42**, 135404 (2009).
[23] F. Ouachtari, A. Rmili, S. El Bachir Elidrissi, A. Bouaoud, H. Erguig, P. Elies, J. Mod. Phys. **2**, 1073 (2011).
[24] L. Zhou, X. Hu, S. Wu, Surf. Coat. Tech. **228**, S171 (2013).
[25] W. G. C. Kumarage, R. P. Wijesundera, V. A. Seneviratne, C. P. Jayalath, B. S. Dassanayake, J. Phys. D: Appl. Phys. **49**, 095109 (2016).
[26] L. Wenyi, C. Xun, C. Qiulong, Z. Zhibin, Mater. Lett. **59**, 1 (2005).
[27] X. H. Zhao, A.X. Wei, Y. Zhao, J. Liu, J. Mater. Sci. Mater. Electron. **24**, 457 (2013).
[28] A. E. Alam, W. M. Cranton, I. M. Dharmadasa, J. Mater. Sci. Mater. Electron. **30**, 4580 (2019).
[29] O. Tuna, Y. Selamet, G. Aygun, L. Ozyuzer, J. Phys. D: Appl. Phys. **43**, 055402 (2010).

[30] R. M. Patrikar, Appl. Surf. Sci. **228**, 213 (2004).
[31] S. Kasap, P. Capper, Handbook Springer of Electronic and Photonic Materials. Springer International Publishing, 2nd Edition, 1450 p., 978–3–319–48931–5 (2017)
[32] M. J. Kim, H. T. Kim, J. K. Kang, D. H. Kim, D. H. Lee, S. H. Lee, S. H. Sohn, Mol. Cryst. Liq. Cryst. **532**, 437 (2010).
[33] I. Horcas, R. Fernández, J. M. Gómez–Rodríguez, J. Colchero, J. Gómez–Herrero, A. M. Baro, Rev. Sci. Instrum. **78**, 013705 (2007).
[34] Image Metrology A/S, Mountains®8 software, Available from world wide web: https://www.digitalsurf.com
[35] U. Sarac, M. C. Baykul, J. Alloys Compd. **552**, 195 (2013).
[36] U. Sarac, M. Kaya, M. C. Baykul, Appl. Phys. A **126**, 239 (2020).
[37] A. Y. Suh, A. A. Polycarpou, T. F. Conry, Wear **255**, 556 (2003).
[38] C. Trapalis, N. Todorova, M. Anastasescu, C. Anastasescu, M. Stoica, M. Gartner, M. Zaharescu, T. Stoica, Thin Solid Films **517**, 6243 (2009).
[39] M. C. Baykul, A. Balcioglu, Microelectron. Eng. **51–52**, 703 (2000).
[40] M. C. Baykul, N. Orhan, Thin Solid Films **518**, 1925 (2010).
[41] A. Y. Jaber, S.N. Alamri, M. S. Aida, Thin Solid Films **520**, 3485 (2012).
[42] Md. S. Hossain, H. Kabir, M. M. Rahman, K. Hasan, M. S. Bashar, M. Rahman, Md. A. Gafur, S. Islam, A. Amri, Z.–Tao Jiang, M. Altarawneh, B.Z. Dlugogorski, Appl. Surf. Sci. **392**, 854 (2017).
[43] S. Chandramohan, A. Kanjilal, J. K. Tripathi, S. N. Sarangi, R. Sathyamoorthy, T. Som, J. Appl. Phys. **105**, 123507 (2009).
[44] A. S. Hassanien, A. A. Akl, Superlattice Microst. **89**, 153 (2016).
[45] A. S. Hassanien, A. A. Akl, J. Alloys Compd. **648**, 280 (2015).